Vortex and Surface Phase Transitions in Superconducting Higher-order Topological Insulators

Sayed Ali Akbar Ghorashi[1], Taylor L. Hughes[2], Enrico Rossi[1]

[1]*Department of Physics, William & Mary, Williamsburg, Virginia 23187, USA and*
[2]*Department of Physics and Institute for Condensed Matter Theory,*
University of Illinois at Urbana-Champaign, IL 61801, USA
(Dated: September 25, 2019)

Topological insulators (TIs) having intrinsic or proximity-coupled s-wave superconductivity host Majorana zero modes (MZMs) at the ends of vortex lines. The MZMs survive up to a critical doping of the TI at which there is a vortex phase transition that eliminates the MZMs. In this work, we show that the phenomenology in higher-order topological insulators (HOTIs) can be qualitatively distinct. In particular, we find two distinct features. (i) We find that vortices placed on the gapped (side) surfaces of the HOTI, exhibit a pair of phase transitions as a function of doping. The first transition is a surface phase transition after which MZMs appear. The second transition is the well-known vortex phase transition. We find that the surface transition appears because of the competition between the superconducting gap and the local $\mathcal{T}$-breaking gap on the surface. (ii) We present numerical evidence that shows strong variation of the critical doping for the vortex phase transition as the center of the vortex is moved toward or away from the hinges of the sample. We believe our work provides new phenomenology that can help identify HOTIs, as well as illustrating a promising platform for the realization of MZMs.

Introduction.–In the past decade there has been an explosion of interest in new forms of topological matter, driven by the discoveries of topological insulators and gapless topological semimetals[1–3]. The search for Majorana zero modes (MZMs) has been at the heart of it, due to its promising applications in developing the building blocks of topological quantum computation[4]. In a seminal work, Fu and Kane[5] showed that a MZM can be trapped in the core of a vortex when an s-wave superconductor proximitizes a TI with gapless, Dirac surface states. Later, Hosur et. al. [6] demonstrated that these MZMs can actually survive up to some critical doping of the TI bulk bands beyond the band edges[7–9].

Recently, some aspects of topological phases of matter have received newborn attention after the introduction of so-called higher-order topological phases [10–15], which has spawned numerous works in the last few years [16–32]. An nth-order topological phase of a system of dimension d possesses gapless boundary modes on the $d-n$ dimensional boundaries with $1 < n \leq d$, unlike a conventional topological phase for which $n = 1$. Since its first theoretical discovery[10], there have been experimental realizations of higher-order topological insulators (HOTIs) in several meta-material contexts [33–36], as well as evidence in solid state electronic materials[12]

In light of this previous work we can ask a natural question: can proximitized (or intrinsically superconducting) 3D HOTIs exhibit MZMs in their vortices? Indeed, since one can arrive at a second-order HOTI in 3D by perturbing a $\mathcal{T}$-invariant topological insulator while preserving the product of C_4^z and $\mathcal{T}$ symmetries [13], then there is a clear connection between this question and Fu and Kane's original work. In this article we answer this question in the affirmative, but reveal the appearance a surface phase transition tuned by changes in the chemical
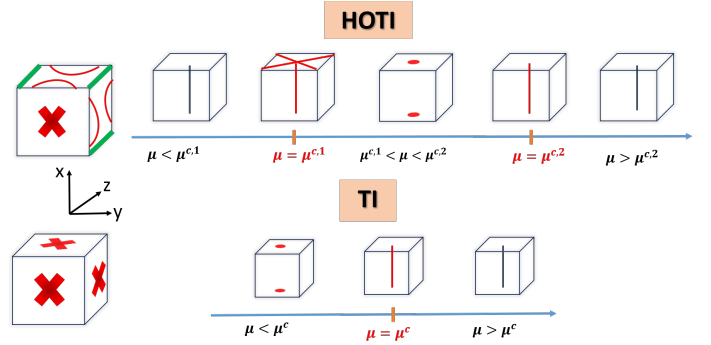

FIG. 1. A schematic picture depicting the evolution of the vortex bound states with doping. The low-energy 1D vortex spectrum can be utilized to distinguish between HOTI (with chiral hinge states) from a conventional TI. By tuning of doping at the critical doping $\mu^{c,1}$, the gapped surfaces of HOTIs undergo a surface phase transition and stable MZMs only appear for $\mu^{c,1} < \mu < \mu^{c,2}$.

potential that distinguishes the HOTI from the ordinary TI phenomenology.

Let us explicitly summarize our findings. We begin with a conventional 3D $\mathcal{T}$-invariant topological insulator. From here, Ref. 13 predicts that one can form a 3D HOTI having chiral hinge states if one adds a $C_4^z \mathcal{T}$ symmetric term. This term acts to gap out the surfaces perpendicular to the x and y directions, but leaves the z-surfaces gapless. When proximitized by s-wave superconductivity, the z-surfaces behave as in an ordinary TI, as long as any vortices are far from any (gapless) hinges of the sample. However, vortices on the side surfaces show a different phenomenology. For weak proximity effect, and for chemical potentials inside the gap of the side surface states, we find that vortices do not trap an odd number of

MZMs. For a fixed proximity-induced pairing strength, one finds two clear critical points as μ is tuned (note we are implicitly assuming $\mu \geq 0$ without loss of generality). Besides the large critical doping $\mu^{c,2}$ that marks the known vortex phase transition (VPT)[6], we find a new lower critical doping $\mu^{c,1}$ (Fig. 1). For chemical potentials smaller than $\mu^{c,1}$ no stable MZMs are bound to vortices on the side surfaces. We will show below that the lower critical point represents a topological surface phase transition where the surface changes from being dominated by a $\mathcal{T}$-breaking gap to a proximity-induced gap. As μ increases through the surface transition the Majorana hinge states are eliminated and we recover the usual TI phenomenology. As such we find that stable, vortex-bound MZMs do exist on the side surfaces for the range $\mu^{c,1} < \mu < \mu^{c,2}$.

Below, we provide more details and describe the surface transition as the competition between the superconducting gap and the $C_4\mathcal{T}$ symmetric term (that induces the surface $\mathcal{T}$-breaking gap) in the HOTI. We further investigate the effect of an external Zeeman term and show that it can be utilized to modify $\mu^{1,c}$ depending on its strength and orientation. We illustrate these transitions, in comparison with an ordinary proximitized TI, in Fig. 1. We believe that our results clearly delineate the vortex phenomenology in proximity induced TIs and HOTIs, and can be employed as a promising approach for identifying HOTIs as well as platform for the realization of MZMs.

Model.– We begin with a lattice model for a 3D HOTI having proximity-induced s-wave singlet pairing. Let us use the the Nambu basis $\Psi_{\mathbf{k}}^T = \left(\psi_{\mathbf{k}}, \psi_{-\mathbf{k}}^\dagger\right)$ where $\psi_{\mathbf{k}}^T = (c_\uparrow, c_\downarrow\, d_\uparrow, d_\downarrow)$ and (c,d) represent different orbitals while $\uparrow / \downarrow$ are spin. The Bogoliubov-de-Gennes (BdG) Hamiltonian for our model is is $H_{SC} = \sum_{\mathbf{k}} \Psi_{\mathbf{k}}^\dagger h_{\mathbf{k}}^{BdG} \Psi_{\mathbf{k}}$ where

$$h_{\mathbf{k}}^{BdG} = \begin{bmatrix} H_{HOTI}(\mathbf{k}) - \mu & \Delta \\ \Delta^* & -H_{HOTI}^T(-\mathbf{k}) + \mu \end{bmatrix} \quad (1)$$

and

$$H_{HOTI}(\mathbf{k}) = \left(M + t_0 \sum_i \cos(k_i)\right) \kappa_z \sigma_0$$
$$+ t_1 \sum_i \sin(k_i)\kappa_x\sigma_i + t_2(\cos(k_x) - \cos(k_y))\kappa_y\sigma_0. \quad (2)$$

The pairing term is $\Delta = \delta_0\kappa_0\sigma_y$ where δ_0 is the strength of the pairing, and κ, σ are Pauli matrices in orbital and spin spaces, respectively. For $t_2 = 0$, Eq. (2), represents the well-known model of 3D time-reversal invariant TI, for $1 < |M| < 3$ (strong TI) and $0 < |M| < 1$ (weak TI). For $t_2 \neq 0$ the system can be in a 3D chiral HOTI phase when the TI is tuned to a strong TI phase[13]. The term proportional to t_2 breaks time-reversal and C_4 rotational symmetry while preserving

their product: $(C_4\mathcal{T})H_{HOTI}^*(k_x, k_y, k_z)(C_4\mathcal{T})^{-1} = H_{HOTI}(k_y, -k_x, -k_z)$, $C_4 = \kappa_0 e^{-i\pi\sigma_z/4}$ and $\mathcal{T} = \kappa_0\sigma_y$. In the presence of superconductivity, either proximity-induced or intrinsic, the HOTI will develop chiral Majorana hinge modes, with a pair of chiral modes on hinges parallel to z that split when they intersect the top and bottom surfaces[37]. Now, we will turn
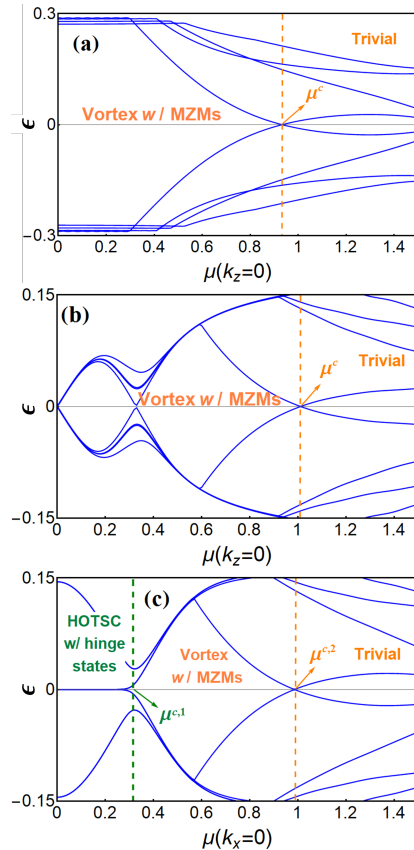

FIG. 2. VPT spectrum versus μ for (a) a TI at $k_z = 0$ having a vortex line parallel to z (b) a HOTI at $k_z = 0$ having a vortex line parallel to z (c) a HOTI at $k_x = 0$ having a vortex line parallel to x. For (a,b) the lattice size is 40×40 in the plane perpendicular to the vortex line. In (c) the lattice size is 100×100. Model parameters $M = -2.5, t_0 = 1, t_1 = 1, t_2 = 1, \delta_0 = 0.3$ are used.

our focus to vortex phenomenology. We can implement a vortex (perhaps better thought of as a vortex line) in a plane (perpendicular to a plane) parameterized by (x_i, x_j) using a spatially dependent pairing term $\Delta(\mathbf{r}) = \Delta \tanh(r/\xi_0)e^{i\phi_0}$, where $r = \sqrt{x_i^2 + x_j^2}$, $\phi_0 = \arctan(x_j/x_i)$, and we choose $\xi_0 = 1$. We ignore any contributions from the vector potential and Zeeman term from the field used to induce the vortex as in Ref. 6. The model for the strong TI has cubic symmetry so inserting a vortex on surfaces normal to $x, y,$ or z gives rise to the same physics. However, this is not the case for HOTIs, as cubic symmetry is broken to an axial symmetry that distinguishes z from x and y. From the

$C_4\mathcal{T}$ symmetry one expects similar behavior for vortices along x and y (up to a time-reversal transformation), but the z-direction can be distinct.

Results.– Following Ref. [6], we obtain the low-energy spectrum in the presence of a vortex by numerically diagonalizing the BdG Hamiltonian in Eq. (1) having periodic boundary conditions in the direction parallel to the vortex line (results are shown in Fig. 2). For easy comparison with earlier results we choose the following set of parameters: $M = -2.5$, $t_0 = t_1 = 1$ (in the remainder all energies are in units of t_0). For this choice of parameters all of the interesting physics is happening near the Γ point so we focus on $k_z = 0$ ($k_x = 0$) for vortex lines parallel to z (x).

For the parameters mentioned above, Ref. [6] showed MZMs at the ends of vortex lines survive up to a critical doping of $\mu^c \sim 0.9$ where the vortex lines undergo a VPT. In Fig. 2(a), we have reproduced this result for comparison. For chemical potentials smaller than μ^c the spectrum on the (periodic) vortex line is gapped, and MZMs will appear if the vortex line is terminated at a surface. From symmetry this result is independent of the orientation of the vortex line, e.g., vortex lines parallel to x or z have the same μ^c.

Next, we turn on t_2 to push the system into the HOTI phase and obtain the spectrum for vortex lines oriented in the z (Fig. 2(b)) and the x (Fig. 2(c)) directions. We find that a critical μ still exists around $\mu \sim 1.0$, for both vortex orientations, having only a small increase compared to the TI case. However, we see a qualitative difference for small chemical potentials, i.e., there are other gapless points in Fig. 2(b,c) that are absent in the case of an ordinary TI. Without a vortex, a HOTI with superconducting pairing as in Eq. (1), is gapped on all surfaces. However, it possesses low-energy Majorana hinge states for a specific range of μ. In Fig. 2(b) the gapless point at $k_z = 0$ and $\mu = 0$ is simply the hinge modes of the proximitized HOTI. As μ is tuned away from zero the hinge states parallel to z have their zero-energy nodal point shifted off $k_z = 0$ so we only see finite-energy states associated to the hinges for $\mu \neq 0$. These hinge modes exist up to around $\mu \sim 0.3$ where there is a surface phase transition.

Now we can consider a vortex line parallel to x with a spectrum shown in Fig. 2(c). Up to $\mu^{c,1}$ (denoted by green vertical dashed line), there are hinge modes, and for this orientation the zero-energy nodal point is not shifted away from $k_x = 0$ as μ is increased. At $\mu^{c,1}$ there is a surface phase transition, after which the hinge states are removed. We show the evolution of the low-energy surface states (without a vortex) in Fig. 3(a-c) as we tune μ through $\mu^{c,1}$. In Fig. 3(e-h) we show the 3D probability densities of low-energy modes when a vortex is present and is oriented along the x direction. In the evolution of the probability densities we first see hinge-states (e)

followed by states extended along the surface (f) at the surface phase transition. After the surface phase transition the MZMs appear (g) which are subsequently destroyed at $\mu^{c,2}$, (h). Remarkably, we see that the MZMs appear only after the surface phase transition. This is in sharp contrast to the surfaces of the TI and the (001) surface of the HOTI as these always host MZMs as long as $\mu < \mu^{c,2}$.

To get a more clear understanding of the surface phase transition demonstrated in Fig. 3, we derive an effective surface Hamiltonian for the (100) surface of the proximitized HOTI by treating the $C_4^z\mathcal{T}$ symmetric term in Eq. (2) perturbatively. We find [See SM],

$$h_{eff}(\mathbf{k}) = v_z k_z \tau_z \sigma_y + v_y k_y \tau_0 \sigma_z - \frac{t_2}{2}\tau_z\sigma_x$$
$$+ \delta_0 \tau_y \sigma_y - \mu\tau_z\sigma_0. \quad (3)$$

From Eq. (3) we see that both the $C_4\mathcal{T}$ symmetric term, and the superconducting pairing, can independently gap out the surface states (since they both fully anticommute with the kinetic energy terms), but they commute with each other, therefore they can be thought of as *competing* masses on the surface. Hence, this can lead to a gap closure at $k_y = k_z = 0$ when $\mu^c = \sqrt{t_2^2 - 4\delta_0^2}/2$. A prediction from this analysis is that a surface phase transition only appears in the $t_2 > 2\delta_0$ regime, i.e., when the local $\mathcal{T}$-breaking surface gap is initially stronger than the proximity-induced gap. Otherwise, we would not expect a surface phase transition to occur, and consequently we would always expect to have MZMs for $\mu < \mu^{c,2}$, similar to the ordinary TI since the proximity gap dominates. Now, to show this more rigorously we compute $\mu^{c,1}$ numerically by varying the t_2 for a fixed δ_0. From Fig. 3(d), we clearly see that, for a fixed superconducting gap δ_0, when increasing t_2, $\mu^{c,1}$ increases in qualitative agreement with the analytical result.

It is always experimentally beneficial to be able to tune phase transitions using various types of external perturbations. We propose that, in addition to the chemical potential, an external Zeeman term can provide some amount of tunability of the surface phase transition. Let us consider a vortex line along the x direction passing through the center of the $y - z$ plane. An external magnetic field B_x in the x direction gives rise to the Zeeman term $B_x J_x = B_x\tau_z\kappa_0\sigma_x$. This term can partially suppress the effect of t_2. To understand this, we project the J_x matrix to the low-energy Hamiltonian on the $y - z$ surface and find $B_x\tau_z\sigma_x$ which is of the same form as the $C_4\mathcal{T}$ symmetric term in Eq. 3. To get a quantitative sense, for our choice of parameters, turning on $B_x = 0.1$, for example, can reduce $\mu^{c,1}$ from 0.33 to 0.16. For sufficiently strong magnetic field, the phase appears after SurfPT can still possess Majorana hinge states. We leave a detailed investigation of the interplay between magnetic field and higher-order
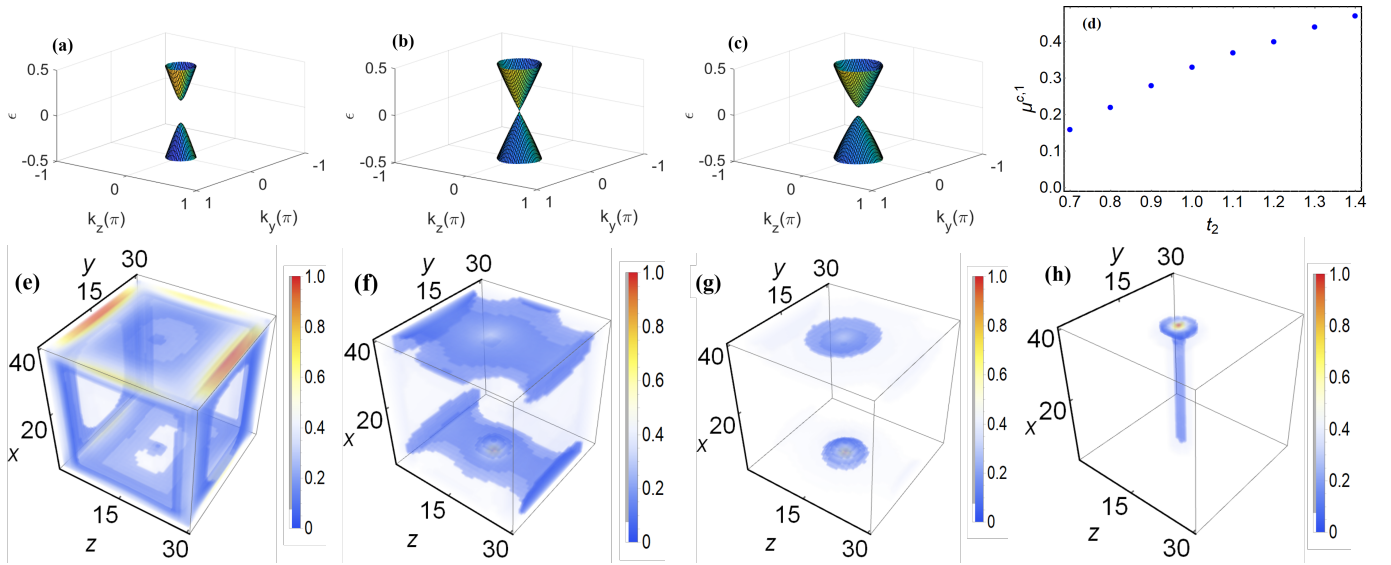
FIG. 3. Surface phase transition in a HOTI in presence of superconductivity. (a-c) The evolution of surface states in the $y-z$ plane for $\mu = 0.1, 0.33, 0.4$, respectively. A surface phase transition occurs at $\mu^{c,1} \sim 0.33$. (d) $\mu^{c,1}$ vs t_2. (e-h) The evolution of the probability density profile of the lowest energy states when a vortex is inserted perpendicular to the $y-z$ surface and μ is tuned. (e) Hinge modes (f) surface phase transition at $\mu^{c,1}$ (g) Majorana zero modes (h) vortex phase transition at $\mu^{c,2}$ We use model parameters $M = -2.5, t_1 = 1, t_2 = 1, \delta_0 = 0.3$. Lattices of size of $40 \times 30 \times 30$ are used to obtain the 3D probability density profiles.

topological superconductivity for elsewhere[38], and keep our focus on the vortex phenomena here. On the other hand, a Zeeman field perpendicular to the vortex line (i.e., parallel to the surface) will not influence $\mu^{c,1}$ on that surface. Therefore, we find that we can tune the surface phase transition on a given surface by applying a Zeeman field. If one has control over the orientation of the field one may be able to selectively tune the critical doping levels on each surface (for example, one may tune opposing surfaces such that one surface has a surface phase transition at finite μ, while the transition on the opposing surface is suppressed to zero by applying a field normal to that surface).

Now, we briefly discuss how the location of the vortex center (V_c) on the side surfaces can impact the critical doping $\mu^{c,2}$. Here, we provide numerical evidence that shows strong variation of $\mu^{c,2}$ as V_c is moved closer to the hinges. For the sake of simplicity we take periodic boundary conditions parallel to the vortex line and position a vortex on the diagonal of the surface plane. Let the distance between the vortex center and the hinge at corner $(1,1)$ be $d_h = (n-1)\sqrt{2}$, and the distance between the vortex center and the center of the plane be $d_c = (N/2 - n)\sqrt{2}$, where the surface is an $N \times N$ square, and n is the coordinate of the vortex center along the diagonal. Fig. 4 shows $\mu^{c,2}$ versus d_h, for two different system sizes, $N = 24, 28$. By changing, the system size, d_c changes but d_h remains same. By decreasing d_h we find $\mu^{c,2}$ increases, but the results are independent of N,

therefore we conclude that the vortex is sensitive to d_h rather than d_c. We note that the details of the variation (and how strong the variation is), are a function of various parameters of the system, and in some cases can be affected more strongly by finite size effects. We note that for a fixed set of system parameters, the variation of d_h only affects $\mu^{c,2}$ and not $\mu^{c,1}$ as the surface physics is nominally insensitive to the presence of the vortex. However, an external Zeeman term could affect results of Fig. 4 indirectly, since the presence/absence/spatial profile of the hinge states are effected by the Zeeman field, and thus the vortex-hinge hybridization can be affected by such a field. While this affect may be difficult to observe with a single (likely pinned) vortex, but may be measureable with a vortex lattice where one might expect a distribution of $\mu^{c,2}$ across the lattice depending on the spatial location of the vortices relative to the hinges.

In summary, we have found that vortex phenomenology can be utilized to distinguish a class of HOTIs from TIs, and can also serve as a platform for the realization of Majorana zero modes. In HOTIs having proximity-induced or intrinsic s-wave superconductivity we identified a new critical doping $\mu^{c,1}$ that marks a topological surface phase transition for the gapped (side) surfaces. We demonstrated that MZMs only appear in a range of doping levels between $\mu^{c,1}$ and $\mu^{c,2}$, the latter of which represents a previously known vortex transition. The surface transition results from two competing mass terms on the gapped surfaces of HOTI: the superconducting gap and a $\mathcal{T}$-breaking mass term resulting from the bulk $C_4 \mathcal{T}$
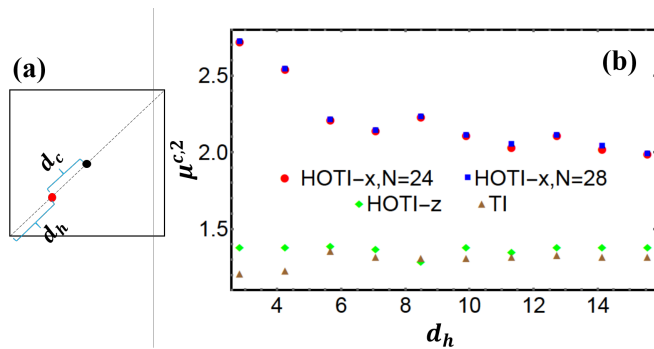
FIG. 4. (a) schematic picture shows the distance between a vortex (red dot) from hinge d_h and center d_c of lattice (black dot), (b)$\mu^{c,2}$ vs d_h for HOTI with superconducting vortex along x-direction (HOTI-x) with two system sizes of $N = 24, 28$ and HOTI-z and TI with $N = 28$. $M = -2, t_1 = 1, t_2 = 1$(HOTI)$, \delta_0 = 0.2$.

symmetric term that is responsible for driving a parent $\mathcal{T}$-invariant TI into the HOTI. The surface phase transition can be tuned with chemical potential or Zeeman fields which may help experimental detection of the phase transitions and MZMs. Recently, iron-based superconductors attracted attention because they can host both topological and trivial vortices simultaneously [39–45]. Here we have shown that the HOTIs are another example of such systems, which for a specific range of dopings and applied Zeeman fields, can host both trivial and topological vortices, but in different orientations. Furthermore, we have provided numerical evidence showing strong variation of the critical doping $\mu^{c,2}$ depending on the spatial location of the vortex center. Possible future research directions would be to repeat the investigations of some of the experimentally known characteristics of MZMs in TI/SC systems but for HOTIs[9]. For example, the spatial distribution of MZMs may be affected by the surface physics discussed here. Also, considering that the side surfaces have competing superconducting and magnetic mass terms, one could ask whether it can affect the spin-selective Andreev reflection profile. We leave these studies to future work.

[1] M. Z. Hasan and C. L. Kane, "Colloquium: Topological insulators," Rev. Mod. Phys. **82**, 3045–3067 (2010).

[2] Xiao-Liang Qi and Shou-Cheng Zhang, "Topological insulators and superconductors," Rev. Mod. Phys. **83**, 1057–1110 (2011).

[3] Ching-Kai Chiu, Jeffrey C. Y. Teo, Andreas P Schnyder, and Shinsei Ryu, "Classification of topological quantum matter with symmetries," Reviews of Modern Physics **88**, 035005 (2016).

[4] Chetan Nayak, Steven H. Simon, Ady Stern, Michael Freedman, and Sankar Das Sarma, "Non-abelian anyons and topological quantum computation," Rev. Mod. Phys. **80**, 1083–1159 (2008).

[5] Liang Fu and C. L. Kane, "Superconducting proximity effect and majorana fermions at the surface of a topological insulator," Phys. Rev. Lett. **100**, 096407 (2008).

[6] Pavan Hosur, Pouyan Ghaemi, Roger S. K. Mong, and Ashvin Vishwanath, "Majorana modes at the ends of superconductor vortices in doped topological insulators," Phys. Rev. Lett. **107**, 097001 (2011).

[7] Ching-Kai Chiu, Matthew J. Gilbert, and Taylor L. Hughes, "Vortex lines in topological insulator-superconductor heterostructures," Phys. Rev. B **84**, 144507 (2011).

[8] Hsiang-Hsuan Hung, Pouyan Ghaemi, Taylor L. Hughes, and Matthew J. Gilbert, "Vortex lattices in the superconducting phases of doped topological insulators and heterostructures," Phys. Rev. B **87**, 035401 (2013).

[9] Hao-Hua Sun and Jin-Feng Jia, "Detection of majorana zero mode in the vortex," npj Quantum Materials **2**, 34 (2017).

[10] Wladimir A Benalcazar, B Andrei Bernevig, and Taylor L Hughes, "Quantized electric multipole insulators." Science **357**, 61–66 (2017).

[11] Wladimir A Benalcazar, B Andrei Bernevig, and Taylor L Hughes, "Selected for a Viewpoint in Physics Electric multipole moments, topological multipole moment pumping, and chiral hinge states in crystalline insulators," Physical Review B **96**, 245115 (2017).

[12] Frank Schindler, Zhijun Wang, Maia G. Vergniory, Ashley M. Cook, Anil Murani, Shamashis Sengupta, Alik Yu. Kasumov, Richard Deblock, Sangjun Jeon, Ilya Drozdov, Hélène Bouchiat, Sophie Guéron, Ali Yazdani, B. Andrei Bernevig, and Titus Neupert, "Higher-order topology in bismuth," Nature Physics **14**, 918–924 (2018).

[13] Frank Schindler, Ashley M. Cook, Maia G. Vergniory, Zhijun Wang, Stuart S. P. Parkin, B. Andrei Bernevig, and Titus Neupert, "Higher-order topological insulators," Science Advances **4**, eaat0346 (2018).

[14] Josias Langbehn, Yang Peng, Luka Trifunovic, Felix von Oppen, and Piet W. Brouwer, "Reflection-symmetric second-order topological insulators and superconductors," Phys. Rev. Lett. **119**, 246401 (2017).

[15] Zhida Song, Zhong Fang, and Chen Fang, "$(d - 2)$-dimensional edge states of rotation symmetry protected topological states," Phys. Rev. Lett. **119**, 246402 (2017).

[16] Sayed Ali Akbar Ghorashi, Xiang Hu, Taylor L. Hughes, and Enrico Rossi, "Second-order dirac superconductors and magnetic field induced majorana hinge modes," Phys. Rev. B **100**, 020509 (2019).

[17] Motohiko Ezawa, "Higher-order topological insulators and semimetals on the breathing kagome and pyrochlore lattices," Phys. Rev. Lett. **120**, 026801 (2018).

[18] Motohiko Ezawa, "Minimal models for wannier-type higher-order topological insulators and phosphorene," Phys. Rev. B **98**, 045125 (2018).

[19] Eslam Khalaf, "Higher-order topological insulators and superconductors protected by inversion symmetry," Phys. Rev. B **97**, 205136 (2018).

[20] Dumitru Călugăru, Vladimir Juričić, and Bitan Roy, "Higher-order topological phases: A general principle of construction," Phys. Rev. B **99**, 041301 (2019).

[21] Majid Kheirkhah, Yuki Nagai, Chun Chen, and Frank Marsiglio, "Majorana corner flat bands in two-dimensional second-order topological superconductors," (2019), arXiv:1904.00990.

[22] Zhongbo Yan, Fei Song, and Zhong Wang, "Majorana corner modes in a high-temperature platform," Phys. Rev. Lett. **121**, 096803 (2018).

[23] Chen-Hsuan Hsu, Peter Stano, Jelena Klinovaja, and Daniel Loss, "Majorana kramers pairs in higher-order topological insulators," Phys. Rev. Lett. **121**, 196801 (2018).

[24] Yuxuan Wang, Mao Lin, and Taylor L. Hughes, "Weak-pairing higher order topological superconductors," Phys. Rev. B **98**, 165144 (2018).

[25] Qiyue Wang, Cheng-Cheng Liu, Yuan-Ming Lu, and Fan Zhang, "High-temperature majorana corner states," Phys. Rev. Lett. **121**, 186801 (2018).

[26] Tao Liu, James Jun He, and Franco Nori, "Majorana corner states in a two-dimensional magnetic topological insulator on a high-temperature superconductor," Phys. Rev. B **98**, 245413 (2018).

[27] Xiaoyu Zhu, "Second-order topological superconductors with mixed pairing," Phys. Rev. Lett. **122**, 236401 (2019).

[28] Rui-Xing Zhang, William S. Cole, and S. Das Sarma, "Helical hinge majorana modes in iron-based superconductors," Phys. Rev. Lett. **122**, 187001 (2019).

[29] S. Franca, D. V. Efremov, and I. C. Fulga, "Phase-tunable second-order topological superconductor," Phys. Rev. B **100**, 075415 (2019).

[30] Zhongbo Yan, "Majorana corner and hinge modes in second-order topological insulator-superconductor heterostructures," (2019), arXiv:1907.02070.

[31] Yi-Ting Hsu, William S. Cole, Rui-Xing Zhang, and Jay D. Sau, "Inversion-protected higher order topological superconductivity in monolayer WTe$_2$," (2019), arXiv:1904.06361.

[32] Song-Bo Zhang and Björn Trauzettel, "Detection of second-order topological superconductors by Josephson junctions," (2019), arXiv:1905.09308.

[33] Christopher W. Peterson, Wladimir A. Benalcazar, Taylor L. Hughes, and Gaurav Bahl, "A quantized microwave quadrupole insulator with topologically protected corner states," Nature **555**, 346–350 (2018).

[34] Jiho Noh, Wladimir A. Benalcazar, Sheng Huang, Matthew J. Collins, Kevin P. Chen, Taylor L. Hughes, and Mikael C. Rechtsman, "Topological protection of photonic mid-gap defect modes," Nature Photonics **12**, 408–415 (2018).

[35] Marc Serra-Garcia, Valerio Peri, Roman Süsstrunk, Osama R. Bilal, Tom Larsen, Luis Guillermo Villanueva, and Sebastian D. Huber, "Observation of a phononic quadrupole topological insulator," Nature **555**, 342–345 (2018).

[36] Stefan Imhof, Christian Berger, Florian Bayer, Johannes Brehm, Laurens W. Molenkamp, Tobias Kiessling, Frank Schindler, Ching Hua Lee, Martin Greiter, Titus Neupert, and Ronny Thomale, "Topolectrical-circuit realization of topological corner modes," Nature Physics **14**, 925–929 (2018).

[37] Raquel Queiroz and Ady Stern, "Splitting the hinge mode of higher-order topological insulators," Phys. Rev. Lett. **123**, 036802 (2019).

[38] Sayed Ali Akbar Ghorashi, Unpublished.

[39] Kun Jiang, Xi Dai, and Ziqiang Wang, "Quantum anomalous vortex and majorana zero mode in iron-based superconductor fe(te,se)," Phys. Rev. X **9**, 011033 (2019).

[40] Elio J. König and Piers Coleman, "Crystalline-symmetry-protected helical majorana modes in the iron pnictides," Phys. Rev. Lett. **122**, 207001 (2019).

[41] Lingyuan Kong, Shiyu Zhu, Michał Papaj, Hui Chen, Lu Cao, Hiroki Isobe, Yuqing Xing, Wenyao Liu, Dongfei Wang, Peng Fan, Yujie Sun, Shixuan Du, John Schneeloch, Ruidan Zhong, Genda Gu, Liang Fu, Hong-Jun Gao, and Hong Ding, "Half-integer level shift of vortex bound states in an iron-based superconductor," Nature Physics 2019 , 1–7 (2019).

[42] Peng Zhang, Zhijun Wang, Xianxin Wu, Koichiro Yaji, Yukiaki Ishida, Yoshimitsu Kohama, Guangyang Dai, Yue Sun, Cedric Bareille, Kenta Kuroda, Takeshi Kondo, Kozo Okazaki, Koichi Kindo, Xiancheng Wang, Changqing Jin, Jiangping Hu, Ronny Thomale, Kazuki Sumida, Shilong Wu, Koji Miyamoto, Taichi Okuda, Hong Ding, G. D. Gu, Tsuyoshi Tamegai, Takuto Kawakami, Masatoshi Sato, and Shik Shin, "Multiple topological states in iron-based superconductors," Nature Physics , 1 (2018).

[43] Shengshan Qin, Lunhui Hu, Xianxin Wu, Xia Dai, Chen Fang, Fu-chun Zhang, and Jiangping Hu, "Topological Vortex Phase Transitions in Iron-Based Superconductors," (2019), arXiv:1901.03120.

[44] Areg Ghazaryan, Pedro L. S. Lopes, Pavan Hosur, Matthew J. Gilbert, and Pouyan Ghaemi, "Effect of Zeeman coupling on the Majorana vortex modes in iron-based topological superconductors," (2019), arXiv:1907.02077.

[45] Gang Xu, Biao Lian, Peizhe Tang, Xiao-Liang Qi, and Shou-Cheng Zhang, "Topological superconductivity on the surface of fe-based superconductors," Phys. Rev. Lett. **117**, 047001 (2016).